

# Comparison of theoretical and experimental red and near infrared absorption spectra in overheated potassium vapour

C. Vadla<sup>1,a</sup>, R. Beuc<sup>1</sup>, V. Horvatic<sup>1</sup>, M. Movre<sup>1</sup>, A. Quentmeier<sup>2</sup>, and K. Niemax<sup>2</sup>

<sup>1</sup> Institute of Physics, Bijenicka 46, 10000 Zagreb, Croatia

<sup>2</sup> ISAS – Institute for Analytical Sciences, Bunsen-Kirchhoff-Strasse 11, 44139 Dortmund, Germany

Received 5 April 2005 / Received in final form 20 June 2005

Published online 30 August 2005 – © EDP Sciences, Società Italiana di Fisica, Springer-Verlag 2005

**Abstract.** The  $K_2$  molecular spectra have been theoretically and experimentally investigated in the wavelength range between 550 nm and 1100 nm and at the temperatures between 650 K and 1100 K. Semi-classical theoretical simulations were performed using the most recent data for the potential energy curves for the  $K(4S)+K(4S)$  and  $K(4S)+K(4P)$  systems and the relevant dipole transition moments. The measurements of the corresponding spectra were performed by a spatially resolved absorption method in an inhomogeneous overheated potassium vapour generated in a heat pipe. Both theoretical and experimental investigations confirmed that the reduced absorption coefficients of the potassium diffuse triplet bands at 575 nm, 721.5 nm and 1095 nm are practically independent of temperature in a wide temperature range. The obtained data for the reduced absorption coefficients of these bands can be used for a simple and accurate determination of potassium atom number densities in the range from  $5 \times 10^{16} \text{ cm}^{-3}$  to  $5 \times 10^{18} \text{ cm}^{-3}$ .

**PACS.** 31.15.Gy Semiclassical methods – 33.20.Ea Infrared spectra – 33.20.Kf Visible spectra – 33.70.Fd Absolute and relative line and band intensities

## 1 Introduction

This work was initially motivated by a need to find a way of accurate spectroscopic determination of the atom number density in a dense potassium vapours (higher than  $10^{16} \text{ cm}^{-3}$ ), which is of particular interest for actual investigations in our laboratory. In distinction from standard spectroscopic methods based on the atomic line absorption, the method explored here is aiming for the possibility of using molecular bands as a standard for the atom number density determination. In general, molecular spectra are dependent on vapour number density and the vapour temperature. Following the quasistatic approximation, the frequency-dependent absorption coefficient of a molecular band is proportional to the square of the atom number density  $N$  and to the Boltzmann factor  $\exp[-\Delta V_l(R)/kT]$ , where the latter includes the energy difference  $\Delta V_l(R) = V_l(R) - V_l(\infty)$  for the lower potential curve at the internuclear separation  $R$ . The molecular bands occurring in the transitions starting from shallow ground states are of particular interest because their absorption coefficients do not depend on temperature ( $|\Delta V_l(R)/kT| \ll 1$ ) and are in fact the functions of the atom number density only.

In the red and infrared spectral region of the potassium molecules, the molecular bands at 575 nm, 712.5 nm and 1095 nm occurring in the transitions from the shallow triplet ground state, appear as possible candidates to be used for the atom number density determination. To theoretically examine and experimentally confirm this assumption, we compared the theoretically simulated and experimentally observed molecular absorption spectra in the region from 550 nm to 1100 nm in a strongly overheated, dense potassium vapour. The investigated molecular bands (with exception of 575 nm band) are related to the transitions between the  $K(4S)+K(4S)$  and  $K(4S)+K(4P)$  interaction potentials, where the most pronounced spectral features are the well-known X–A and X–B molecular bands, which emerge in the singlet transitions  $X^1\Sigma_g^+ \rightarrow A^1\Sigma_u^+$  and  $X^1\Sigma_g^+ \rightarrow B^1\Pi_u$ , respectively. Theoretical simulations of the  $K_2$  absorption spectra have been performed using the most recent but unpublished [1] data for the potential curves and the corresponding dipole transition moments as well as recent data available in the literature for the potential curves [2]. The particular contributions to the absorption coefficient were calculated applying the semi-classical approach described in [3]. In the simple quasistatic approximation, the classical absorption spectra generally agree with the overall quantum mechanical band shapes, except for nearly periodic band structures and non-classical behaviour at the

<sup>a</sup> e-mail: vadla@ifs.hr

satellite positions. The present refined treatment of the spectra, based on uniform Airy approximation, avoids singularities pertinent to the quasistatic line shapes and takes into account interferences among contributions of various Condon points. The presented comparison between the measured and the calculated shapes of molecular spectra at various atomic number densities and, especially, at various temperatures serves as a sensitive check for the accuracy of the interaction potentials used in the simulation.

If the investigated metal vapour is in equilibrium with the metal bath, the number density and the temperature are in fixed relationship, which is defined by the vapour pressure curve and the state equation for an ideal gas. In order to measure the spectra at nearly constant particle number density and in a wide temperature range, the vapour should be overheated, which, in principle, is easy to do when working with cells. However, when dealing with dense alkali vapours at temperatures higher than 800 K, the use of the heat pipe is the simplest solution, but in this case the realisation of the sufficient overheating is not a simple technical problem [4]. In contrast to usual solutions for vapour overheating in the heat pipe, in this work we applied a simple arrangement which allows spatially resolved absorption measurements and spectroscopic investigation of alkali vapours in the range between the arbitrary chosen temperature of the liquid bath to an overheating temperature  $T$  of about 1200 K.

## 2 Theory

Within the semiclassical approach [3], the absorption coefficient is given by

$$k(T, \omega) = N^2 \frac{2\pi\omega}{3chg_i} \sum_{\alpha, \beta} \langle |C_{\alpha\beta}(E, b, \omega)|^2 \rangle_{E, b}, \quad (1)$$

where  $N$  is the atom number density,  $g_i$  is the statistical weight of the initial state, while the summation extends over all degenerate substates of the initial  $|i, \alpha\rangle$  and final  $|f, \beta\rangle$  states for which optical transitions are contributing to the absorption spectra in the wavelength region of interest. The brackets  $\langle \dots \rangle_{E, b}$  denote the averaging over collisions energies  $E$  at a temperature  $T$  and summation over the impact parameters  $b$ . The amplitude  $C(E, b, \omega)$  is of the form of the Fourier transform describing a time dependent classical oscillator:

$$C(E, b, \omega) = \int_{-\infty}^{\infty} D(R(t)) e^{i\varphi(E, b, \omega) - i\omega t} dt, \quad (2)$$

where  $D(R(t))$  is electronic transition moment and the time dependent phase is expressed as

$$\varphi(E, b, \omega, t) = \frac{1}{\hbar} \int_{-\infty}^t \Delta V(R(E, b, t')) dt', \quad (3)$$

with  $\Delta V$  and  $R$  representing the difference potential involved and (time dependent) internuclear distance, respectively.

Using the simple stationary-phase argument, one easily obtains the quasistatic formula [3, 5], which reads as follows:

$$k(\lambda, T) = N^2 \frac{4\pi^3 e^2 \hbar}{mc} \sum_{\alpha, \beta} \sum_C \frac{R_C^2 f_{\alpha\beta}(R_C)}{|\Delta' V_{\alpha\beta}(R_C)|} \times \exp \{ -(V_{\alpha}(R_C) - V_{\alpha}(\infty)) / k_B T \}. \quad (4)$$

For each transition  $\alpha \rightarrow \beta$ , there is a corresponding difference potential  $\Delta V_{\alpha\beta} = V_{\alpha} - V_{\beta}$ , its first derivative  $\Delta' V_{\alpha\beta}$ , and the molecular oscillator strength  $f_{\alpha\beta}$ . The latter is proportional to the statistical weight of the initial substate and to the square of the corresponding electronic transition moment. The second summation is over all Condon points  $R_C$  which, for the given transition, satisfy the classical Franck-Condon condition  $\Delta V_{\alpha\beta} = hc/\lambda$ .

The relation (4) is valid in the region of energies for which there are no extrema in the difference potential curve. In the neighbourhood of an extreme two Condon points come close together and derivatives of the difference potentials tend to zero producing a non-physical singularity. However, as described in details in [3], the method of uniform mapping can be applied yielding to a formula which describes contribution to the spectrum due to the coalescent pair of Condon points which correctly takes into account the interference among them and avoids the singularity.

Considering the manifolds of the interaction potential curves stemming from  $4^2S + 4^2S$  and  $4^2S + 4^2P$  asymptotes we have taken into account all transitions which give contributions to the absorption in the wavelength region of interest.

In the major part of the theoretical simulations presented here we used ab initio potential energy functions and the relevant dipole transition moments from reference [1], where about 50 electronic states have been investigated by all-electron self-consistent field (SCF) and full valence configuration interaction (CI) calculations using carefully saturated Gaussian-type orbitals (GTO) basis sets and including the effective core polarization potential (CPP). Where comparison with experiment was possible, Yan and Meyer [6] have found out agreement to within  $30\text{--}80\text{ cm}^{-1}$  for the excitation energies and to better than  $1\text{ cm}^{-1}$  for vibrational frequencies. Figure 1 shows the potential curves taken from reference [1], the relevant differential potentials, and the corresponding contributions to the calculated absorption spectrum. The results for the reduced absorption coefficient  $k/N^2$  at  $T = 750\text{ K}$  are depicted in the right part of Figure 1. The satellite bands around 720 nm, 1050 nm, and 1100 nm correspond to the extrema of  $1^3\Pi_g \rightarrow x^3\Sigma_u^+$ ,  $A^1\Sigma_u^+ \rightarrow X^1\Sigma_g^+$ , and  $1^3\Sigma_g^+ \rightarrow x^3\Sigma_u^+$  difference potentials, respectively.

For the simulations of the spectra we have also used the recent potentials published by Magnier et al. [2]. Unfortunately, these results [2] were not accompanied with the corresponding calculations of the transition dipole

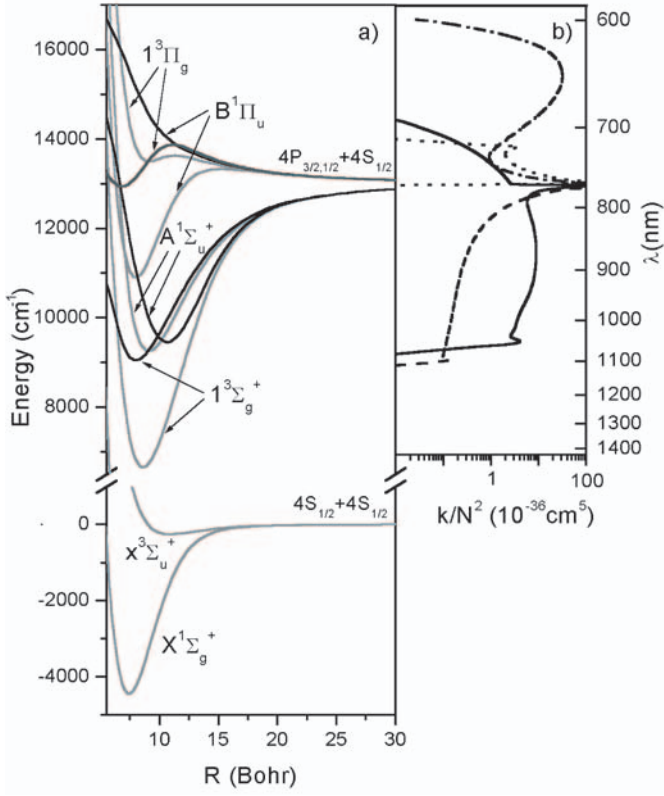


**Fig. 1.** Left part: potential curves of the  $K_2$  molecule in the ground and first excited states. The calculated potentials taken from [1] are given by grey curves, while the black curves depict the differential potentials. Right part: contributions to the reduced absorption coefficient given in the logarithmic scale and calculated for the temperature  $T = 750$  K; solid line: A–X band; dashed-dotted line: B–X band; dashed line:  $1^3\Sigma_g^+ - x^3\Sigma_u^+$ ; dotted line:  $1^3\Pi_g - x^3\Sigma_u^+$ . See text for further details.

moments. Therefore, in the spectra simulations based on the potentials from [2] we used the dipole moments given in [1].

In order to test the applied semiclassical approach alone, we have also used available experimentally determined potential functions for the singlet transitions. For the  $X^1\Sigma_g^+$ ,  $A^1\Sigma_u^+$ , and  $B^1\Pi_u$  states we have used data from Amiot et al. [7,8], Manaa et al. [9], and Heinze et al. [10], respectively. The points in the inner portion of the potential well were generated by a fit to an exponential of the form  $Ae^{-BR}$ , where  $A$  and  $B$  are parameters, and  $R$  is the internuclear distance. At larger  $R$  we have smoothly joined data to the long-range form calculated by Marinescu and Dalgarno [11]. Finally, we have constructed the potential curves as a cubic spline fit generated from the data. As for the triplet states, analogous test using the experimentally determined pair  $x^3\Sigma_u^+$  and  $1^3\Sigma_g^+$  could not be carried out because, to our knowledge, experimental data are available in literature only for the ground state [12,13]. For the sake of simplicity, we introduce here the abbreviations YM, MAA for the theoretical potentials reported in [1,2], while the ES and

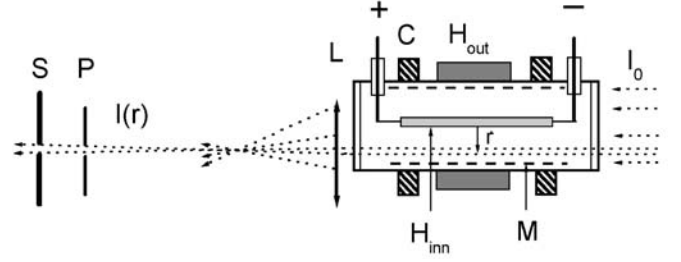


**Fig. 2.** Experimental arrangement for spatially resolved absorption measurements. See text for further explanations. S – monochromator slit, P – pinhole, L – lens, C – cooling, H – heaters, M – mesh.

ET label the experimental singlet [7–10] and experimental triplet [12,13] potentials, respectively. In all simulations we used the transition dipole moments calculated by Yan and Meyer [1].

### 3 Experimental

The experimental arrangement is schematically shown in Figure 2. By the use of an outer heater (resistance:  $40 \Omega$ ) the potassium vapour (vapour column length:  $6.5 \pm 0.5$  cm) was generated in the central zone of the stainless-steel heat pipe having the inner diameter of 20 mm and the length of 18 cm. Re-circulation of the liquid potassium was accomplished by a mesh. Argon was used as a buffer gas. The potassium vapour was overheated with a help of an inner heater built-in along the heat pipe axis. This heater was a  $250 \mu\text{m}$  thick molybdenum wire wound up in helix form with an outer diameter of 2 mm and 12 cm in length. The resistance of helix-heater was  $2 \Omega$ . Molybdenum was found to be the most suitable material for the present purpose, because of its resistance to hot and dense potassium vapours.

With maximum heating power of the outer heater (500 W) it was possible to reach potassium vapour pressure of 200 mbar. However, it is known that in alkali vapours at pressures higher than about 20–30 mbar, a turbulent cluster fog is formed in the transition regions between the hot vapour column and the cold buffer-gas zones. Additionally, the web-like structured solidification of potassium takes place in these regions, which completely obstructs optical path through the heat pipe after several hours of working at high pressures. This problem does not exist if absorption cells are used. However, there are no cells with optical windows which can tolerate potassium vapour at temperatures above 800 K. Therefore, the use of a heat pipe is the only adequate technical solution. The inner heater, which is longer than the vapour column, has a double function. First, it turned out that, clogging in the cold zone and the formation of turbulent fog of small droplets at the hot-cold boundaries can be completely suppressed at high potassium pressure conditions (above 50 mbar) if the inner heater is run at moderate power ( $\approx 5$  W). At such conditions, the potassium vapour

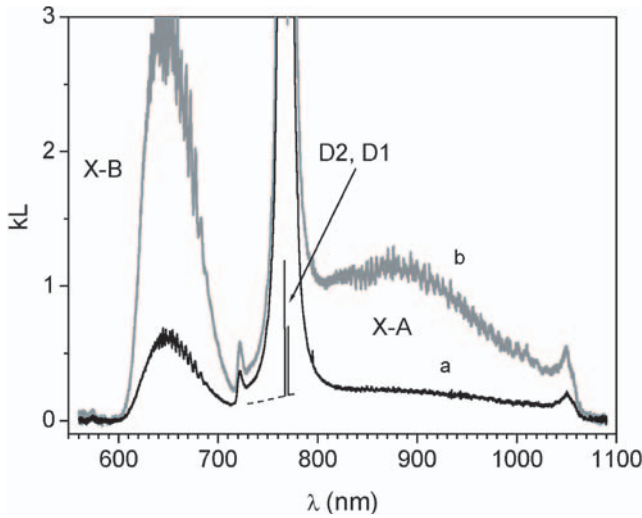


**Fig. 3.** Measured optical depths  $kL$  in strongly overheated potassium vapour at positions  $r = 2$  mm (a) and  $r = 7$  mm (b) from the axis of the heat pipe.

near the heat pipe axis is slightly overheated, and the temperature at the heat pipe axis is about 50–100 K higher than the temperature of the metal bath in the mesh at the heat pipe wall. On the other hand, with maximum inner heating power ( $\approx 25$  W) a strongly overheated vapour is produced. Now, the radial temperature distribution is ranging from  $T_C \approx 1200$  K at the heat pipe axis to the bath temperature  $T_W$  at the heat pipe wall.  $T_W$  is mainly dependent on the outer heating system. It has to be emphasized that with an increase of the outer heating, i.e. with an increase of the potassium vapour pressure, the thermal conductivity of the heat pipe also increases, which results in significant cooling of the inner heating wire.

Spatially resolved absorption measurements were performed as illustrated in Figure 2. The absorption zone was illuminated with a collimated white-light beam (intensity:  $I_0(\lambda)$ ) of a halogen lamp and imaged by a lens (focal length: 15 cm) with a 2:1 ratio onto a screen with a pinhole (diameter: 0.5 mm). The screen was placed at a distance of 3 cm in front of the monochromator slit (slit width: 0.2 mm). By moving the heat pipe in radial direction, the absorption in thin columns (thickness  $dr < 1$  mm) at different distances  $r$  from the heat pipe axis was measured by recording the transmitted intensity  $I(r, \lambda)$  in the region of the overheated vapour. Typical absorption spectra obtained with spatial, i.e. temperature resolution, are shown in Figure 3.

The measurements were performed using a 0.5 m Jarrel-Ash monochromator and a RCA 7102 photomultiplier (S-1 cathode) cooled thermoelectrically down to  $-20$  °C. The collected data were stored on a laboratory PC. These measurements were made at potassium number densities in the range between  $5 \times 10^{16}$  cm $^{-3}$  and  $2 \times 10^{17}$  cm $^{-3}$ , and in the overheating temperature interval from 650 K to 1100 K.

In absorption measurements with high spatial resolution there is a competition between spatial resolution and

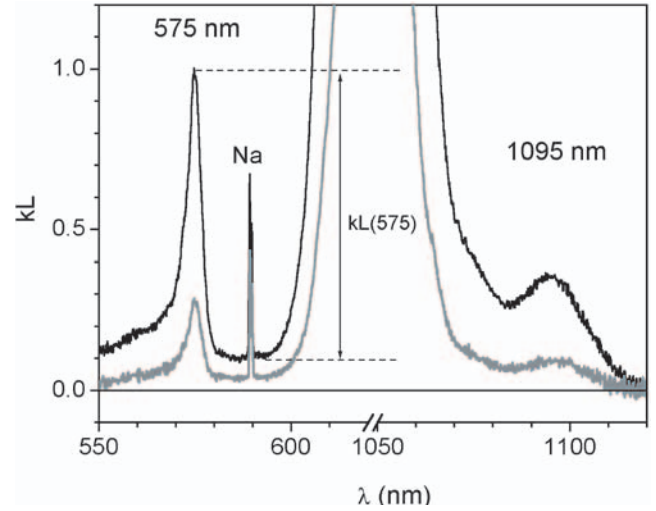


**Fig. 4.** Spatially unresolved measurements of the optical depths at the average potassium number densities  $N = 3.2 \times 10^{17}$  cm $^{-3}$  (grey line) and  $N = 6.1 \times 10^{17}$  cm $^{-3}$  (black line). The corresponding average temperatures are  $T = 870$  K and  $T = 940$  K, respectively.

detection sensitivity, because an increase of spatial resolution always means a reduction of the diameter of the incident beam and, therefore, of the radiation intensity. In particular, this was a problem for the measurements in the wavelength region around 1100 nm, i.e. at the infrared edge of the spectral response of the photomultiplier used. In order to maintain the necessary sensitivity, the measurements in that particular region were performed without spatial resolution. Here, the overall absorption across the whole cross-section of the vapour column was measured and the transmitted beam was focused directly onto the monochromator entrance slit. These measurements were performed at potassium densities up to  $10^{18}$  cm $^{-3}$  and the vapours were slightly overheated, just to minimize the cluster perturbations.

Typical spectra obtained in this part of the measurement are presented in Figure 4. In addition, for the reasons which are explained in the text below, the spatially unresolved absorption spectra were also measured during the heat pipe cooling cycle. These transient spectra (not shown here) were recorded using an Échelle-spectrometer (ESA 3000 by LLA, Berlin) equipped with an intensified charge-coupled device (ICCD), in order to simultaneously obtain absorption spectra of the whole wavelength region of interest.

## 4 Comparison of experimental and theoretical results

### 4.1 Quantitative analysis of the experimental spectra

The atom number densities in the particular temperature zone were determined by absorption measurements in the wings of the potassium D lines. For the evaluation we used

a very reliable method based on a detailed theoretical and experimental analysis which has been described in [14]. According to [14], the absorption coefficient  $k^{blue}$  in the blue wing of the resonance doublet can be expressed as:

$$k^{blue}(\Delta\lambda) = 3.9 \times 10^{-34} P(Y) \frac{N^2}{[\Delta\lambda(\text{nm})]^2}, \quad (5)$$

where  $k^{blue}$  is given in  $\text{cm}^{-1}$ ,  $N$  in  $\text{cm}^{-3}$ ,  $\Delta\lambda$  is the detuning from the D2 line centre, and  $P(Y)$  is the polynomial defined by:

$$P(Y) = 3.0752 + 1.8476Y - 0.0508Y^2 + 0.2278Y^3 - 0.0253Y^4. \quad (6)$$

Here,  $Y = \Delta\lambda/\Delta_{fs}$  with  $\Delta_{fs} = 3.4$  nm being the fine structure splitting of the potassium resonance doublet. The relation (6) is valid for  $1 \text{ nm} \leq \Delta\lambda \leq 10 \text{ nm}$ .

The molecular background in the range of the resonance line wings was approximated by a straight line (dashed line in Fig. 3) and subtracted from the measured data. The parameters of the straight line (height and the slope of the background) were varied until the remaining  $kL$  vs.  $\Delta\lambda$  acquired the same wavelength dependence as given by relations (5) and (6). The atom number density  $N(r)$  at the radial distance  $r$  from the heat pipe axis was determined with an accuracy of about 3% taking into account the  $kL$  values obtained, the estimated vapour column length  $L = (6.5 \pm 0.5)$  cm, and relation (5). The measurements of the absorption coefficient were performed from the inner heater up to a position near to the heat pipe wall. The number density  $N(r_w)$  just above the liquid metal in the mesh at the heat pipe wall was determined by the extrapolation of the  $N(r)$  data set. The outer and inner heating powers were 220 W and 10 W, respectively. The heating gas pressure was 15 mbar. The potassium atomic number densities  $N(r)$  varied from  $N(r_h) = (1.11 \pm 0.03) \times 10^{17} \text{ cm}^{-3}$  near the edge of the inner heater to the extrapolated value  $N(r_w) = (1.55 \pm 0.05) \times 10^{17} \text{ cm}^{-3}$  at the heat pipe wall. Since the potassium vapour at the heat pipe wall is in thermal equilibrium with the liquid metal, the corresponding temperature  $T(r_w)$  can be determined by use of atomic vapour pressure curve [15] combined with the relation between the pressure, number density and the temperature for an ideal gas. The value found was  $T(r_w) = (727 \pm 5)$  K. According to [15], the pressure of the potassium molecules at this temperature amounts to about 1% of the total vapour pressure. Therefore, it can be safely neglected in comparison with the pressure of the atomic vapour. Then, by use of the ideal gas law, the temperature at particular distance  $r$  can be determined using the simple relation  $T(r) = T(r_w)N(r_w)/N(r)$ .

In Figure 5, the measured spectra and their theoretical simulations are given in the form of the reduced absorption coefficient  $k_R = k(\lambda, T)/N^2$  for four different temperatures. The theoretical simulations presented in Figure 5 used the hybrid ES+YM potentials, i.e. the combination of experimentally determined potential curves of the singlet states and the calculated potential curves of the triplet states.

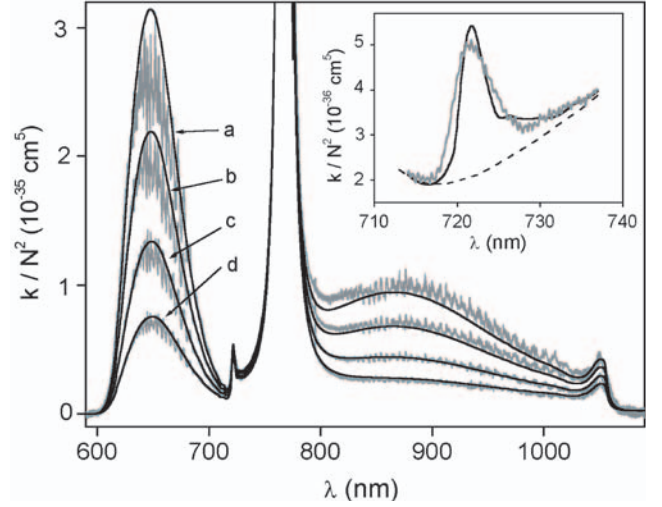


**Fig. 5.** Comparison of experimental (grey lines) and calculated (black lines) reduced absorption coefficient for four different temperatures. Theoretical simulations are performed using the experimental singlet potentials and YM triplet potentials. The experimentally determined temperatures are  $T_a^{Exp} = 880$  K,  $T_b^{Exp} = 925$  K,  $T_c^{Exp} = 960$  K, and  $T_d^{Exp} = 1025$  K (the accuracy of temperature determination:  $\pm 30$  K). The optimum fitting temperatures are  $T_a^{Fit} = 870$ ,  $T_b^{Fit} = 915$  K,  $T_c^{Fit} = 985$  K, and  $T_d^{Fit} = 1080$  K. Inset: the experimental (grey line) and calculated (black line) diffuse band at 721.5 nm for  $T_a^{Exp} = 880$  K. The dashed line represents the estimated molecular background.

## 4.2 Resonance line wings

The wings of the potassium resonance lines are rather insensitive to temperature variation, because they arise from transitions in the long-range interaction region where the potentials are weak and the corresponding Boltzmann factor is close to unity for the temperatures used in the experiment. As one can see in Figure 5, there is an excellent quantitative agreement between the experimental and theoretical results in the region close to the centre of gravity of the potassium resonance lines. This confirms the consistency of the present calculations and the calculations reported in [5], which have been focused on the details in that region only and yielded equations (5) and (6).

## 4.3 Molecular X–A and X–B bands

The extended red wing of the resonance doublet overlaps with the X–A molecular band, which ends as a pronounced “head of the heads” satellite with a peak at 1050 nm. Towards shorter wavelengths there is a diffuse band at 721.5 nm followed by the molecular X–B band. The shapes of both molecular bands are strongly temperature dependent. The temperature dependences of these bands are different because the maxima of the bands originate from different internuclear distances (see Fig. 1) and consequently the X–A and X–B transitions are characterized by different Boltzmann factors. The temperatures taken for the

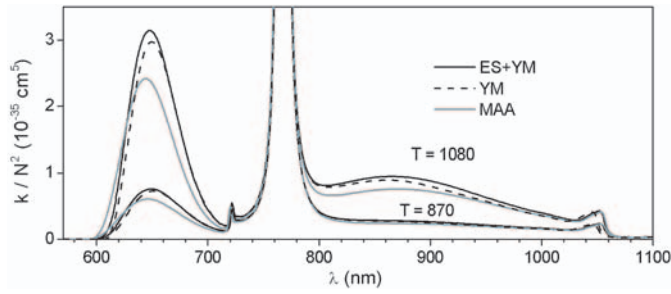


**Fig. 6.** Comparison of the absorption coefficients calculated using the hybrid ES+YM potentials, and the pure theoretical (YM and MAA) potentials for two temperatures.

calculations of the theoretical spectra were compromise values for which the simulations yielded the best fit to the experimental molecular bands. Nevertheless, the compromise temperatures yielded calculated spectra, which were systematically below the experimental spectra in the region of the X–A band. The higher the temperature, the larger is the difference. Contrary to the case of X–A band, the calculated X–B band for the compromise-fit temperatures appears systematically more intense than the experimental band, and the difference is more pronounced as the temperature raises. It should be emphasized that a temperature change of only 10 K significantly deteriorates the agreement between calculated and experimental spectra.

The high sensitivity to temperature variations is due to the fact that besides the contributions from the long-range region, there is also a contribution to the absorption coefficient arising from transitions at short-range internuclear distances, as can be seen from Figure 1. Recently, the same argument was successfully applied for simultaneous determination of temperature and number density of rubidium vapours [16].

The overall agreement between calculated and measured X–A and X–B band shapes is satisfactory. Since the potential energy curves used for calculations of X–A and X–B band absorption were experimentally determined, the results presented in Figure 5 confirm the accuracy of the applied semiclassical approach for calculation of the contributions to the total absorption coefficient. The remaining systematic difference between calculated and observed spectra is probably attributable to the uncertainty of the dipole transition moments used in the calculations, and present results lead us to the conclusion that the YM B–X dipole transition moment is slightly overestimated, while the A–X dipole transition moment is underestimated.

Figure 6 shows the comparison between the spectra obtained using hybrid ES+YM potentials and those calculated using exclusively theoretical YM and MAA potentials. The depths of the potential minima of the singlet ground state for MAA, YM and ES potential curves are  $4331.9 \text{ cm}^{-1}$ ,  $4395.2 \text{ cm}^{-1}$  and  $4450.7 \text{ cm}^{-1}$ , respectively. These differences in the potential minima, i.e. correspondingly different Boltzmann factors, represent the

main cause of the discrepancy among the calculated absorption coefficients. As can be seen in Figure 6, in the major part of the investigated spectral region, the absorption coefficients calculated using the pure YM potentials are much closer to the results obtained with ES + YM potentials than those which were obtained for the case of the MAA potentials. The X–B band calculated via YM potentials is shifted towards red region, while the correspondingly calculated X–A and the “head of the heads” bands are shifted towards blue, which is the consequence of the deviation of the differential potentials from the real ones. On the other hand, compared with the ES + YM case, the MAA potentials result with blue and red shift for the X–B and X–A band, respectively. The simulation based on the MAA potentials yields an excellent agreement with the ES + YM simulation at the red side of the X–A band, especially in the region of the “head of the heads” band, pointing to the fact that the differential MAA potentials in the corresponding region are very good. The detailed account of the theoretical simulations in the mentioned spectral region is given in Section 4.5.

#### 4.4 Diffuse band at 721.5 nm

The experimental and theoretical results of the reduced absorption coefficient at wavelengths around 721.5 nm obtained for the lowest temperature applied are shown in more detail in the inset of Figure 5. The diffuse band at that wavelength belongs to the triplet transition  $x^3\Sigma_u^+ \rightarrow 1^3\Pi_g$  (see Fig. 1). As can be seen from Figure 5, the theoretical curve matches up well with the experimental data, whereas the calculated and measured peak positions are in excellent agreement.

We recall that the triplet contributions to the spectra depicted in Figure 5 were calculated using the triplet YM potentials. The absorption coefficient around 721.5 nm was also calculated using various available potentials and the results are plotted in Figure 7. Besides the hybrid ES+YM potentials, we simulated the spectra with MAA as well as with the hybrid ET+YM potentials. As can be seen in Figure 7, the curves corresponding to the ES+YM and ET+YM potentials are lying very close to each other. This is due to fact that in both simulations the same upper  $1^3\Pi_g$  potential (YM) was used. The maxima of both simulations are very close to 721.5 nm. The simulation of the spectra based on the MAA potentials is quite distinct and yields the position of the maximum of this triplet band which significantly differs from the experiment. Since the position of the maximum is essentially determined by the differential potential, this disagreement points to the inaccuracy of the latter in the case of MAA potentials. The small difference observable between ES+YM and ET+YM calculations of the absorption coefficient is the consequence of the corresponding small difference between theoretical (YM) and experimentally determined (ET) potential curve for the  $x^3\Sigma_u^+$  ground state. This is illustrated in Figure 8, where YM, ET and MAA  $x^3\Sigma_u^+$  potentials are compared. Here, it should be noted that

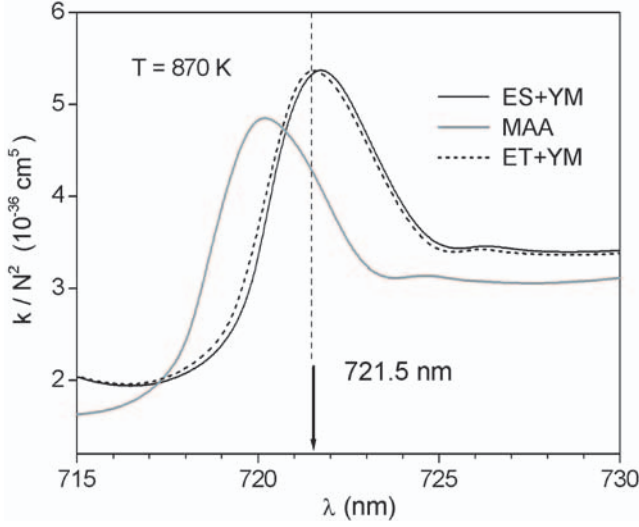


**Fig. 7.** Comparison of calculated absorption spectra around 721.5 nm using various sets of potential energy curves. The arrow marks the maximum of the experimental spectrum.

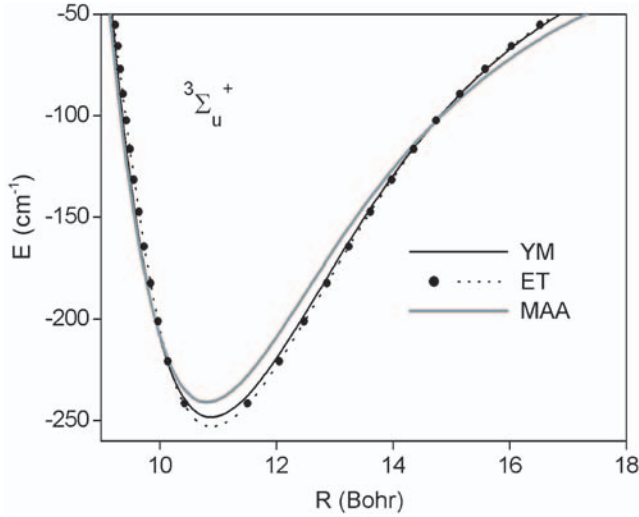


**Fig. 8.** Comparison of the potential energy curves for the ground  $x^3\Sigma_u^+$  state used in the simulations which are presented in Figure 7.

for ET data we have used the RKR points from reference [12], while the energy has been corrected in accordance with reference [13]. The depths  $D_e$  of the potentials are  $252.78\text{ cm}^{-1}$ ,  $248.24\text{ cm}^{-1}$  and  $240\text{ cm}^{-1}$  for the ET, YM and MAA potentials, respectively.

In the present experiment it was found that the reduced absorption coefficient of the 721.5 nm band is temperature independent in a wide temperature range. This band lies on a background related to the X-B band as well as to the X-A band and its temperature independence is due to fact that it originates from the shallow triplet minimum. The absorption coefficient was measured relative to the blue wing of the resonance doublet. In this way the uncertainties of the vapour column

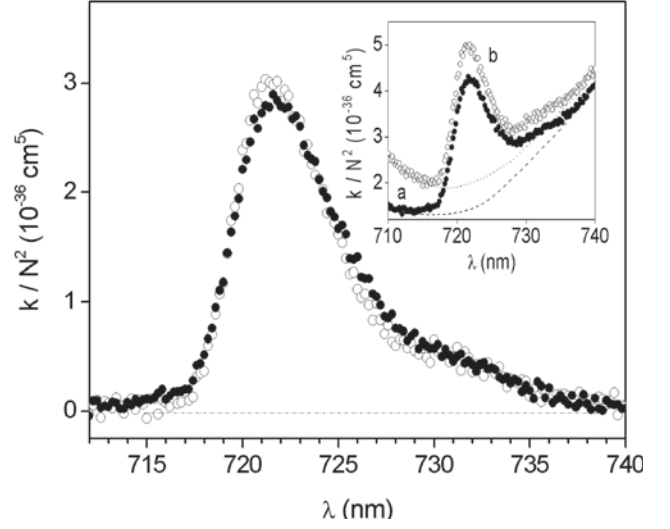


**Fig. 9.** Experimentally determined reduced absorption coefficient of the 721.5 nm band with the background subtracted. The open circles represent the measurement at  $N = 1.1 \times 10^{17}\text{ cm}^{-3}$  and  $T = 1010\text{ K}$ . The full circles represent the data obtained at  $N = 1.3 \times 10^{17}\text{ cm}^{-3}$  and  $T = 870\text{ K}$ . The inset shows original spectra with estimated background (dashed and dotted line).

length cancelled out. The reduced absorption coefficient peak of the 721.5 band obtained by the subtraction of the estimated background (see Fig. 9) was found to be  $k_R(721.5) = (2.9 \pm 0.2) \times 10^{-36}\text{ cm}^5$  for the temperatures in the range from 700 K to 1100 K.

Due to its temperature independence and because the background continuum can be determined by a simple procedure, this band can be very conveniently used for the measurement of the potassium number density.

In this way with the absorption column length of  $\sim 10\text{ cm}$ , typical in spectroscopic experiments, it is easy to measure the potassium number densities between  $2 \times 10^{16}\text{ cm}^{-3}$  and  $2 \times 10^{17}\text{ cm}^{-3}$ . The use of the 721.5 nm band for the potassium number density determination is especially convenient for higher densities where the procedure via resonance wing measurements becomes inaccurate because of the strong molecular background.

#### 4.5 Band at 1095 nm

According to our calculations, the weak band due to the triplet transition  $x^3\Sigma_u^+ \rightarrow 1^3\Sigma_g^+$  appears at about 1100 nm (see right part of Fig. 1). As mentioned in Section 1, this part of the spectrum, which is at the infrared edge of the spectral response of the S1-photomultiplier, was not analyzed using the imaging arrangement with spatial resolution. With the overall absorption across the whole cross-section of the heat pipe and with the transmitted light beam focused onto the monochromator, the investigated infrared triplet band becomes detectable at potassium number densities higher than  $2 \times 10^{17}\text{ cm}^{-3}$ .

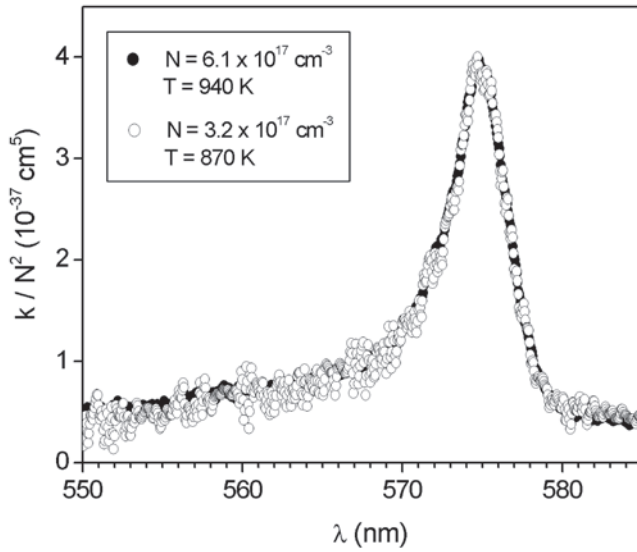


**Fig. 10.** The reduced absorption coefficient of the potassium diffuse band at 575 nm. See text for further explanations.

Figure 4 shows spectra measured at two different number densities above that value. In order to achieve a stable absorption column without cluster perturbations, the potassium vapour was moderately overheated (outer heating power: 300 W, inner heating power: 5 W). This means that the spectra displayed in Figure 4 are related to kinds of average number densities and average temperatures. At present conditions, the absorption is almost 100% in the wavelength range between 600 and 900 nm, so that the potassium atom number density could not be determined neither using the resonance wing nor the 721.5 nm band as standards. However, in the present case the diffuse band with the peak intensity at 575 nm, which is also shown in Figure 4, can be utilized for the atom number density determination. This band occurs in the transition between the triplet interaction potential curves  $^3\Sigma_u^+$  and  $2^3\Pi_g$ , where the upper state is stemming from the K(4S) + K(3D) asymptotes [17, 18]. Since the 721.5 nm and 575 nm bands originate from the same lower state, one can expect that they exhibit similar temperature behaviours.

The reduced absorption coefficient for the 575 nm diffuse band is shown in Figure 10. The displayed data were obtained from the spectra shown in Figure 4.

The reduced absorption coefficient of the 575 nm band was determined by the calibration using the 721.5 nm band. For that reason, the 721.5 and 575 nm bands were measured simultaneously by the spatially resolved absorption method. This particular measurement was performed again in the strongly overheating regime at potassium number densities in the range between  $1 \times 10^{17} \text{ cm}^{-3}$  and  $2 \times 10^{17} \text{ cm}^{-3}$ . It was found that the reduced absorption coefficient of the diffuse 575 nm band, measured with respect to the flat absorption continuum around the sodium resonance doublet, does not depend on the vapour temperature in the range between 750 K and 1100 K. The total peak value (including the flat continuum) for

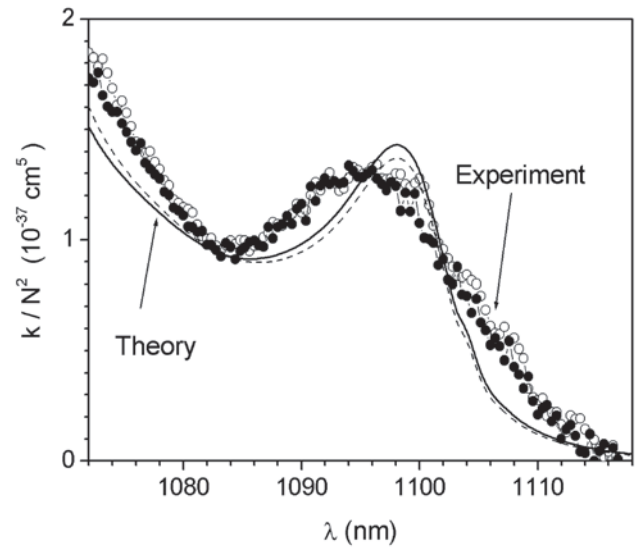


**Fig. 11.** Experimental and theoretical reduced absorption coefficients for the infrared satellite band at 1100 nm. The experimental values are derived from the data displayed in Figure 4. The open and full circles correspond to the measurements at potassium number densities  $N = 3.2 \times 10^{17} \text{ cm}^{-3}$  and  $N = 6.1 \times 10^{17} \text{ cm}^{-3}$ , respectively. The theoretical curves are calculated for  $T = 870 \text{ K}$  (dashed line) and  $940 \text{ K}$  (full line).

the reduced absorption coefficient  $k_R(575)$  amounts to  $(3.9 \pm 0.3) \times 10^{-37} \text{ cm}^5$ .

Using the 575 nm diffuse band as a standard for the potassium number density determination, the spatially resolved absorption measurements yielded the information about the actual physical conditions in the heat pipe, which are related to the spectra given in Figure 4. The average potassium number densities in the measurements shown in Figure 4 were  $3.2 \times 10^{17} \text{ cm}^{-3}$  and  $6.1 \times 10^{17} \text{ cm}^{-3}$ , while the estimated average temperatures were 870 K and 940 K, respectively. The values for  $N$  and  $T$  at the axis and at the heat pipe wall differed about 10% from the average values. The reduced absorption coefficient in the region around 1100 nm is displayed in Figure 11 together with the theoretical simulations. The theoretical simulations were carried out for experimentally determined average temperatures and taking the ES+YM potentials into account.

The definite assignment of the 1095 nm band to the lowest triplet transition was reported in [19] where calculations of the band using the potential energy curves of [17] were also given. The theoretical position of the band maximum was about 1140 nm and the calculated band shape was much broader than the experimentally observed. Several years later, Jeung and Ross [20] published new ab initio potential energy curves for  $\text{K}_2$ , which have been used for recalculation of the spectrum around 1100 nm [21]. This recalculation yielded the theoretical position of the band maximum at 1105 nm. In the present work the agreement between the theory (with ES+YM potentials used) and experiment is much better regarding both the shape and position of the band, as can be seen in Figure 11. The

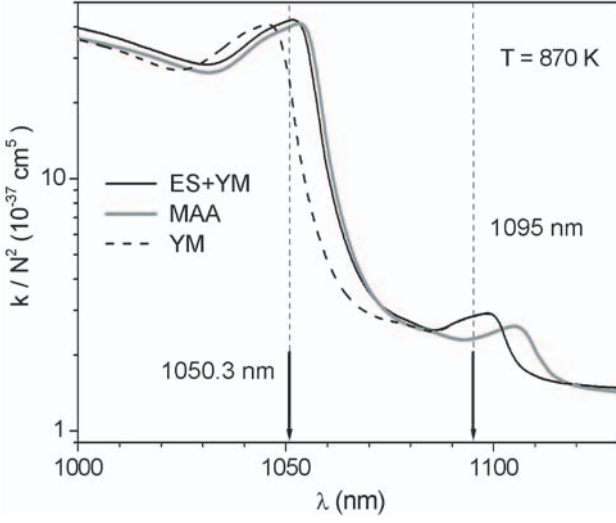


**Fig. 12.** The reduced absorption coefficient calculated using the hybrid ES+YM potentials and the pure theoretical MAA and YM potentials. The maxima of the “head of the heads” at 1050.3 nm and the band at 1095 nm are indicated by black arrows and dashed lines.

comparison of the absorption coefficient calculations carried out using ES+YM, MAA and YM potentials is shown in Figure 12. The displayed spectra include the “head of the heads” at 1050.3 nm and the band at 1095 nm.

In the vicinity of 1050.3 nm band where the spectrum is dominantly determined with singlet X–A transition, the simulation based on MAA potentials almost coincides with the one obtained with ES+YM potentials, which indicates that the MAA differential potential in the region of the corresponding internuclear distances is very good. The use of pure YM potentials resulted with spectrum which deviates substantially from the results obtained with ES+YM and MAA potentials and yields poor agreement with the experimentally determined position of the extremum of the singlet transition. In the region of the 1095 nm band the ES+YM and YM simulations gave the same result because here only the triplet contribution plays role, and for that both simulations rely on the same YM potentials. These simulations are in good agreement with the experiment. The minimum of the differential potential for  $x^3\Sigma_u^+ \rightarrow 1^3\Sigma_g^+$  transition occurs at about 8 Bohr. This is the region of the repulsive triplet ground state where the experimental spectroscopic data are lacking and therefore the comparison with the ET simulation was not made. The position of the 1095 nm band in the simulation using MAA potentials is noticeably shifted towards IR which indicates that differential potential is not accurate enough.

#### 4.6 Continuum between the 575 nm band and the X–B band

According to the theoretical calculations, the absorption of the X–B blue wing decreases rapidly and vanishes below 600 nm (see Fig. 1). On the other hand, at relatively

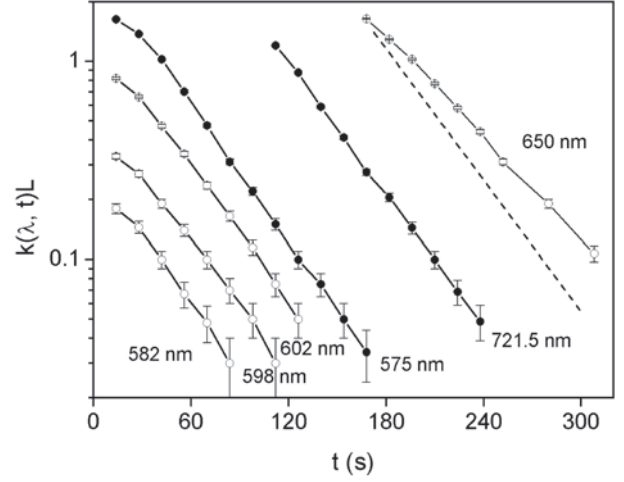


**Fig. 13.** Transient optical depths  $k(\lambda, t)L$  measured during the heat pipe cooling cycle at particular wavelengths of interest. The dashed line indicates the slope of the absorption at the maxima of the triplet bands.

low number densities the potassium vapour is practically transparent in the region around 590 nm which is very convenient for fitting the transmitted intensity  $I(\lambda)$  to  $I_0(\lambda)$ . Nevertheless, at higher potassium number densities a significant continuous absorption appears in that region (see Fig. 4). This continuum has been observed by many groups (see [18] and references therein), but its origin is still unexplained.

To investigate this region in more detail, we have performed measurements of the potassium absorption spectra while cooling the heat pipe. For that purpose an Échelle monochromator was used to record the complete spectrum between 300 and 800 nm simultaneously in time intervals of 14 seconds starting from the moment when the outer heater of the heat pipe was turned off. These measurements were performed without spatial selectivity and with moderate overheating, i.e. in the same way as described in Section 4.5. The starting conditions were defined by the buffer gas pressure of  $p = 160$  mbar and heat pipe mode. The obtained transient values for  $k(\lambda, t)$  at wavelengths of particular interest are plotted in Figure 13.

The data in Figure 13 show that the absorption ratio of the 575 nm and 721.5 nm bands is constant ( $\approx 8$ ) independent of the cooling cycle. Using the temperature independent and known values of  $k_R(575)$  and  $k_R(721.5)$  the corresponding  $N(t)$  and  $T(t)$  at a given time  $t$  can be easily obtained from the vapour pressure curve. As can be seen in Figure 13, the absorption coefficient at 650 nm (peak of the X–B band) decreases slower than those at 721.5 nm and 575 nm, i.e. slower than  $N^2(t)$ . This is due to the Boltzmann factor  $\exp(-\Delta V_i/kT(t))$ . Indeed, from the ratio  $k(650)/k(721.5)$  one can easily check that the Boltzmann plot yields the value for  $\Delta V_i$ , which is, within the error bars, very close to the known depth of the X  $^1\Sigma_g^+$  potential curve.

**Table 1.** The reduced absorption coefficient of the triplet potassium band at 721.5 nm (in units  $10^{-36} \text{ cm}^5$ ) as a function of wavelength.

$\lambda$ (nm)	$k_R^{721.5}$						
710	0.015	718	0.487	726	1.250	734	0.286
710.2	0.015	718.2	0.600	726.2	1.180	734.2	0.266
710.4	0.019	718.4	0.759	726.4	1.124	734.4	0.248
710.6	0.020	718.6	0.912	726.6	1.064	734.6	0.233
710.8	0.020	718.8	1.061	726.8	1.000	734.8	0.220
711	0.020	719	1.236	727	0.945	735	0.208
711.2	0.022	719.2	1.435	727.2	0.885	735.2	0.195
711.4	0.025	719.4	1.651	727.4	0.837	735.4	0.182
711.6	0.028	719.6	1.834	727.6	0.795	735.6	0.171
711.8	0.030	719.8	2.037	727.8	0.760	735.8	0.159
712	0.034	720	2.220	728	0.725	736	0.150
712.2	0.040	720.2	2.410	728.2	0.694	736.2	0.140
712.4	0.044	720.4	2.571	728.4	0.675	736.4	0.133
712.6	0.044	720.6	2.681	728.6	0.656	736.6	0.127
712.8	0.044	720.8	2.790	728.8	0.635	736.8	0.121
713	0.047	721	2.860	729	0.618	737	0.114
713.2	0.053	721.2	2.900	729.2	0.605	737.2	0.107
713.4	0.056	721.4	2.917	729.4	0.592	737.4	0.100
713.6	0.058	721.6	2.921	729.6	0.578	737.6	0.095
713.8	0.059	721.8	2.910	729.8	0.565	737.8	0.089
714	0.062	722	2.890	730	0.553	738	0.084
714.2	0.064	722.2	2.840	730.2	0.541	738.2	0.082
714.4	0.067	722.4	2.788	730.4	0.532	738.4	0.080
714.6	0.071	722.6	2.730	730.6	0.524	738.6	0.075
714.8	0.077	722.8	2.663	730.8	0.515	738.8	0.070
715	0.084	723	2.570	731	0.503	739	0.063
715.2	0.089	723.2	2.473	731.2	0.488	739.2	0.061
715.4	0.093	723.4	2.380	731.4	0.473	739.4	0.060
715.6	0.098	723.6	2.296	731.6	0.460	739.6	0.059
715.8	0.104	723.8	2.207	731.8	0.449	739.8	0.058
716	0.105	724	2.118	732	0.439	740	0.057
716.2	0.108	724.2	2.030	732.2	0.427		
716.4	0.119	724.4	1.930	732.4	0.413		
716.6	0.132	724.6	1.850	732.6	0.396		
716.8	0.147	724.8	1.756	732.8	0.379		
717	0.165	725	1.668	733	0.363		
717.2	0.195	725.2	1.570	733.2	0.349		
717.4	0.240	725.4	1.481	733.4	0.336		
717.6	0.321	725.6	1.400	733.6	0.322		
717.8	0.399	725.8	1.330	733.8	0.305		

Figure 13 also shows that the variation of the absorption coefficient in the far blue wing of the X–B band, for instance at 602 nm, is practically the same as of the triplet bands. This part of the spectrum originates from potassium atoms with high relative kinetic energy at small internuclear distances and it continues smoothly towards the shorter wavelengths. The present measurement suggests that the investigated continuum below 600 nm belongs to the X–B band, which means that it emerges from transitions during collisions of very fast atoms at very short distances. By scaling to the  $k_R(575)$  value, the reduced absorption coefficient of the investigated continuum at 582 nm  $k_R(582)$  was found to be  $(3.7 \pm 0.6) \times 10^{-38} \text{ cm}^5$ . It should be stressed that this datum was used for fitting the transmitted spectrum to the spectrum of the incident light in the absorption measurements described in Section 4.5.

## 5 Discussion

Molecular spectral features belonging to the potassium transitions between the potentials with 4S+4S and 4S+4P asymptotes have been the subject of intensive theoretical and experimental investigations for many years. The triplet bands emerging in this manifold are supposed to be convenient standards for spectroscopic determination of atom number densities in dense potassium vapour. In order to prove this assumption, we performed the theoretical and experimental investigation of the potassium molecular spectra in the red and infrared region. The absorption measurements were performed in the overheated potassium vapour because the molecular spectra are strongly temperature dependent.

**Table 2.** The reduced absorption coefficient of the triplet potassium band at 575 nm (in units  $10^{-37} \text{ cm}^5$ ) as a function of wavelength.

$\lambda$ (nm)	$k_R^{575}$						
550	0.489	559	0.690	568	1.027	577	2.031
550.2	0.491	559.2	0.695	568.2	1.041	577.2	1.841
550.4	0.494	559.4	0.703	568.4	1.059	577.4	1.647
550.6	0.496	559.6	0.711	568.6	1.081	577.6	1.464
550.8	0.497	559.8	0.714	568.8	1.108	577.8	1.302
551	0.505	560	0.715	569	1.137	578	1.166
551.2	0.504	560.2	0.714	569.2	1.163	578.2	1.060
551.4	0.505	560.4	0.718	569.4	1.192	578.4	0.958
551.6	0.505	560.6	0.722	569.6	1.226	578.6	0.862
551.8	0.506	560.8	0.725	569.8	1.262	578.8	0.785
552	0.511	561	0.730	570	1.305	579	0.729
552.2	0.510	561.2	0.734	570.2	1.331	579.2	0.685
552.4	0.508	561.4	0.736	570.4	1.381	579.4	0.640
552.6	0.511	561.6	0.736	570.6	1.440	579.6	0.607
552.8	0.517	561.8	0.739	570.8	1.510	579.8	0.566
553	0.524	562	0.742	571	1.585	580	0.547
553.2	0.527	562.2	0.744	571.2	1.659	580.2	0.529
553.4	0.530	562.4	0.751	571.4	1.741	580.4	0.521
553.6	0.531	562.6	0.755	571.6	1.819	580.6	0.512
553.8	0.535	562.8	0.757	571.8	1.903	580.8	0.501
554	0.543	563	0.762	572	2.001	581	0.494
554.2	0.547	563.2	0.768	572.2	2.093	581.2	0.492
554.4	0.549	563.4	0.770	572.4	2.188	581.4	0.490
554.6	0.554	563.6	0.776	572.6	2.271	581.6	0.486
554.8	0.560	563.8	0.781	572.8	2.379	581.8	0.483
555	0.573	564	0.789	573	2.511	582	0.479
555.2	0.581	564.2	0.801	573.2	2.665	582.2	0.478
555.4	0.585	564.4	0.809	573.4	2.837	582.4	0.473
555.6	0.590	564.6	0.817	573.6	3.008	582.6	0.469
555.8	0.595	564.8	0.826	573.8	3.187	582.8	0.462
556	0.601	565	0.831	574	3.416	583	0.459
556.2	0.608	565.2	0.845	574.2	3.626	583.2	0.456
556.4	0.615	565.4	0.855	574.4	3.801	583.4	0.449
556.6	0.623	565.6	0.866	574.6	3.915	583.6	0.440
556.8	0.628	565.8	0.878	574.8	3.945	583.8	0.435
557	0.636	566	0.891	575	3.925	584	0.429
557.2	0.641	566.2	0.904	575.2	3.870	584.2	0.427
557.4	0.648	566.4	0.916	575.4	3.773	584.4	0.426
557.6	0.656	566.6	0.929	575.6	3.570	584.6	0.418
557.8	0.660	566.8	0.943	575.8	3.378	584.8	0.414
558	0.670	567	0.956	576	3.120	585	0.413
558.2	0.672	567.2	0.972	576.2	2.915		
558.4	0.675	567.4	0.986	576.4	2.688		
558.6	0.683	567.6	0.999	576.6	2.456		
558.8	0.686	567.8	1.012	576.8	2.226		

First we checked the applied semi-classical approach using the experimentally determined potential curves [7–10] for singlet transitions generating the X–A and X–B bands and the theoretical potential curves for the triplet states [1]. In general, the simulation showed good overall agreement with the experimental reduced absorption coefficients of the X–A and X–B bands in the temperature region between 700 K and 1100 K, and, therefore, confirmed the validity of the semi-classical approach. However, there are small differences, particularly in the vicinity of the band maxima, where the interference effects of

the contributions of multiple Condon points become important. The agreement with the experimental spectra depends not only on the semi-classical formula but also on the used dipole moments. Thus, based on these results the definite reason of the observed small differences cannot be found. Nevertheless, the overall agreement between calculated and measured spectra confirms the validity of the applied semi-classical approximation and allows making a statement on the quality of the theoretical potentials, especially on the triplet states for which the agreement with the experiment is excellent.

**Table 3.** The reduced absorption coefficient of the triplet potassium band at 1095 nm (in units  $10^{-37} \text{ cm}^5$ ) as a function of wavelength.

$\lambda$ (nm)	$k_R^{1095}$						
1072	1.800	1084	0.969	1096	1.289	1108	0.451
1072.4	1.770	1084.4	0.968	1096.4	1.285	1108.4	0.416
1072.8	1.733	1084.8	0.970	1096.8	1.280	1108.8	0.381
1073.2	1.704	1085.2	0.975	1097.2	1.273	1109.2	0.347
1073.6	1.672	1085.6	0.981	1097.6	1.263	1109.6	0.322
1074	1.639	1086	0.990	1098	1.250	1110	0.292
1074.4	1.603	1086.4	1.000	1098.4	1.234	1110.4	0.263
1074.8	1.566	1086.8	1.012	1098.8	1.214	1110.8	0.238
1075.2	1.529	1087.2	1.026	1099.2	1.190	1111.2	0.215
1075.6	1.491	1087.6	1.041	1099.6	1.162	1111.6	0.196
1076	1.454	1088	1.057	1100	1.131	1112	0.180
1076.4	1.418	1088.4	1.075	1100.4	1.098	1112.4	0.160
1076.8	1.383	1088.8	1.093	1100.8	1.061	1112.8	0.145
1077.2	1.349	1089.2	1.111	1101.2	1.023	1113.2	0.130
1077.6	1.316	1089.6	1.130	1101.6	0.985	1113.6	0.116
1078	1.283	1090	1.150	1102	0.946	1114	0.102
1078.4	1.251	1090.4	1.169	1102.4	0.908	1114.4	0.087
1078.8	1.220	1090.8	1.187	1102.8	0.871	1114.8	0.071
1079.2	1.190	1091.2	1.205	1103.2	0.835	1115.2	0.055
1079.6	1.160	1091.6	1.222	1103.6	0.797	1115.6	0.038
1080	1.131	1092	1.237	1104	0.766	1116	0.021
1080.4	1.103	1092.4	1.251	1104.4	0.737		
1080.8	1.077	1092.8	1.262	1104.8	0.702		
1081.2	1.054	1093.2	1.272	1105.2	0.673		
1081.6	1.033	1093.6	1.280	1105.6	0.644		
1082	1.014	1094	1.286	1106	0.614		
1082.4	0.999	1094.4	1.289	1106.4	0.584		
1082.8	0.987	1094.8	1.292	1106.8	0.552		
1083.2	0.978	1095.2	1.292	1107.2	0.520		
1083.6	0.972	1095.6	1.291	1107.6	0.486		

In the next step, the reduced absorption coefficients were simulated taking into account the theoretical potentials only, i.e. the triplet as well as the singlet potential curves calculated by Yan and Meyer [1]. These theoretical spectra showed practically the same temperature effects as with the experimentally determined potential curves. Nevertheless, the X–A and X–B band maxima are now slightly shifted to shorter and longer wavelengths, respectively. As for the triplet states, the agreement with the experiment is excellent, particularly in the case of 721.5 nm band. Furthermore, we performed the same procedure with the most recent potential curves which can be found in the literature. These potentials, reported by Magnier et al. [2], yielded an excellent agreement with the experimental findings in the case of singlet transitions in the infrared part of the spectrum. Nevertheless, the singlet contributions in the rest of the spectrum (towards blue) due to potentials from reference [1] fit much better to the experiment than those from reference [2]. Generally, the potentials calculated by Yan and Meyer [1] yield a significantly better agreement with the experimental spectra when they are compared with the simulations based on potentials of Magnier et al. [2].

As for the triplet bands at 575 nm and 721.5 nm the presented theoretical and experimental investigations showed that they can be used for a straightforward and

accurate determination of the potassium number density up to  $5 \times 10^{18} \text{ cm}^{-3}$ . It was found out that the reduced absorption coefficients of these bands do not depend on the temperature in a broad temperature range taking into account the experimental error bars. Therefore, the reduced absorption coefficients can be normalized to the reduced coefficients of the quasistatic wings of the resonance line which have been confirmed as an accurate standard for the determination of the alkali number densities [14]. The values we obtained in this way for  $k_R(721.5)$  and subsequently for  $k_R(575)$ , yielded  $k_R(1095)$  which was in very good agreement with the calculations. This agreement also confirms the self-consistency of the performed evaluation procedure. To make these data easily accessible for possible application, the tabulated values of the reduced absorption coefficient of the triplet potassium bands at 575, 721.5 and 1095 nm are given in Tables 1–3. The data in Tables 1–3 are obtained by averaging and smoothing the experimental results displayed in Figures 9, 10 and 11, respectively.

The band at 575 nm was already recognized by Johnson and Eden [18] as a reliable standard for the determination of potassium number density. According to [18]  $k_R(575)$  amounts to  $2 \times 10^{-37} \text{ cm}^5$  and is constant in the potassium number density range from  $1 \times 10^{17} \text{ cm}^{-3}$  to  $4 \times 10^{17} \text{ cm}^{-3}$ . The value for  $k_R(575)$  reported in [18] is

about two times smaller than our present result. However, as declared by Johnson and Eden in reference [22], the value of the reduced absorption coefficient at 575 nm published in [18] was measured to within a factor of 2 due to the systematic error in the determination of  $N$  (factor of  $\sqrt{2}$ ). The measurements reported in [18] were performed in a cell with the cold finger and the potassium number densities were determined by measuring the temperatures and using the vapour pressure curve. As explained by the authors, the declared error in  $N$  is due to the uncertainty in the temperatures and the long time required to equilibrate metal-vapour in the absorption cell. Although the sign of the systematic error in  $N$  was not specified, it can be concluded from the other details given in [18,22] that the reported value ( $k_R(575) = 2 \times 10^{-37} \text{ cm}^5$ ) was underestimated.

The band at 721.5 nm was also investigated in [18] and the total reduced absorption coefficient  $k_R^{tot}(721.5)$  (including the corresponding X-A and X-B background) was scaled to the  $k_R(575)$ . As shown in [18], the  $k_R^{tot}(721.5)$  decreases with the increase of  $N$ , which is obviously due to strong temperature dependence of the background contributions. With this background subtracted, the ratio  $k_R(721.5)/k_R(575)$  deduced from the data given in [18] is constant ( $\sim 8$ ) and temperature independent which is in excellent agreement with the results reported here.

## 6 Conclusion

The validity of the presented semiclassical calculations of the reduced absorption coefficients has been proven in the case of simulations of the molecular spectra of the K(4S)+K(4S) and K(4S)+K(4P) system. Also, this semiclassical approach presented itself as a reliable mechanism for testing the quality of the calculated potential curves and relevant transition dipole moments.

In addition, the obtained data have shown that the temperature independent reduced absorption coefficients of the potassium diffuse triplet bands can be used for a simple and accurate determination of potassium atom number densities in the range from  $5 \times 10^{16} \text{ cm}^{-3}$  to  $5 \times 10^{18} \text{ cm}^{-3}$ .

The authors would like to express their sincere thanks to Prof. Dr. W. Meyer at the University of Kaiserslautern, Germany, for the access to his results prior to publication, and for

providing them with additional relevant information. Financial support by the Ministry of Science, Education and Sports of the Republic of Croatia, the Ministry of Science and Research (North Rhine-Westphalia) and the Ministry of Education, Science, Research and Technology (FR of Germany) is gratefully acknowledged.

## References

1. L. Yan, W. Meyer, manuscript in preparation
2. S. Magnier, M. Aubert-Frécon, A.R. Allouche, J. Chem. Phys. **121**, 1771 (2004)
3. R. Beuc, V. Horvatic, J. Phys. B: At. Mol. Opt. Phys. **25**, 1497 (1992)
4. S. Milosevic, R. Beuc, G. Pichler, Appl. Phys. B **41**, 135 (1986)
5. M. Movre, G. Pichler, J. Phys. B: At. Mol. Opt. Phys. **13**, 697 (1980)
6. W. Meyer, private communications
7. C. Amiot, J. Mol. Spectrosc. **147**, 370 (1991)
8. C. Amiot, J. Vergès, C.E. Fellows, J. Chem. Phys. **103**, 3350 (1995)
9. M.R. Manaa, A.J. Ross, F. Martin, P. Crozet, A.M. Lyyra, Li Li, C. Amiot, T. Bergeman, J. Chem. Phys. **117**, 11208 (2002)
10. J. Heinze, U. Schühle, F. Engelke, C.D. Caldwell, J. Chem. Phys. **87**, 45 (1987)
11. M. Marinescu, A. Dalgarno, Phys. Rev. A **52**, 311 (1995)
12. L. Li, A.M. Lyyra, W.T. Luh, W.C. Stwalley, J. Chem. Phys. **93**, 8452 (1990)
13. G. Zhao, W.T. Zemke, J.T. Kim, B. Ji, H. Wang, J.T. Bahns, W.C. Stwalley, L. Li, A.M. Lyyra, A.C. Amiot, J. Chem. Phys. **105**, 7976 (1996)
14. V. Horvatic, R. Beuc, M. Movre, C. Vadla, J. Phys. B: At. Mol. Opt. Phys. **26**, 3679 (1993)
15. A.N. Nesmeyanov, *Vapor pressure of the chemical elements*, edited by R. Gray (Elsevier, Amsterdam-London-New York, 1963)
16. D. Aumiler, T. Ban, R. Beuc, G. Pichler, Appl. Phys. B **76**, 859 (2003)
17. D.D. Konowalow, J.L. Fish, State University of New York (personal communications)
18. D.E. Johnson, J.G. Eden, J. Opt. Soc. Am. B **2**, 721 (1985)
19. J. Huennekens, S. Schaefer, M. Ligare, W. Happer, J. Chem. Phys. **80**, 4794 (1984)
20. G.H. Jeung, A.J. Ross, J. Phys B **21**, 1473 (1988)
21. M. Ligare, J.B. Edmonds, J. Chem. Phys. **95**, 3857 (1991)
22. D.E. Johnson, J.G. Eden, J. Chem. Phys. **82**, 2927 (1985)